

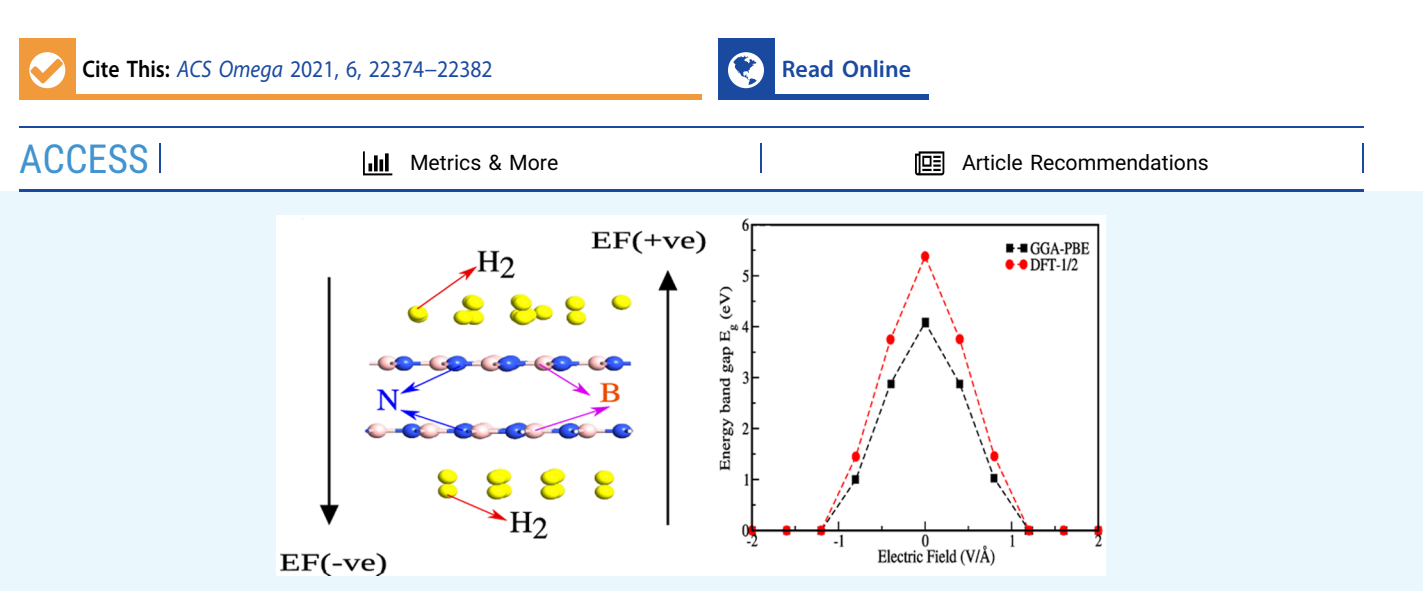


http://pubs.acs.org/journal/acsodf

Article

Enhanced H₂ Storage Capacity of Bilayer Hexagonal Boron Nitride (h-BN) Incorporating van der Waals Interaction under an Applied External Electric Field

Bhanu Chettri, Prasanta Kumar Patra, Sunita Srivastava, Amel Laref, and Dibya Prakash Rai*



ABSTRACT: Lightweight two-dimensional materials are being studied for hydrogen storage applications due to their large surface area. The characteristics of hydrogen adsorption on the h-BN bilayer under the applied electric field were investigated. The overall storage capacity of the bilayer is 6.7 wt % from our theoretical calculation with $E_{\rm ads}$ of 0.223 eV/H₂. The desorption temperature to remove the adsorbed H₂ molecules from the surface of the h-BN bilayer system in the absence of an external electric field is found to be \sim 176 K. With the introduction of an external electric field, the $E_{\rm ads}$ lies in the range of 0.223–0.846 eV/H₂ and the desorption temperature is from 176 to 668 K. Our results show that the external electric field enhances the average adsorption energy as well as the desorption temperature and thus makes the h-BN bilayer a promising candidate for hydrogen storage.

INTRODUCTION

Fossil fuels, which dominate the entire world of energy sources, have major drawbacks due to their high contribution to environmental pollution and global warming due to the emission of CO₂ and other harmful pollutants. Hydrogen can be an alternative to fossil fuels, as it is abundant in nature, has high energy density, and does not emit any harmful pollutants under combustion and hence it is a highly efficient energy carrier. The quest for lightweight solid-state materials for hydrogen storage is at its peak, as the conventional storage techniques have some major drawbacks. For a material to be an efficient hydrogen storage media, there are certain benchmark criteria set up by the United States Department of Energy: gravimetric density should be greater than 6.0 wt % and average adsorption energy ~0.2-0.8 eV per H₂. Twodimension materials such as graphene, silicene, borophene, MoS₂, and so forth are lightweight materials advantageous for offering a high gravimetric density and providing a large surface area, which is suitable for more number of hydrogen molecule adsorption. 1-7 The abovementioned studies also suggested that hydrogen molecules have low binding affinity on pure systems, and thus the possibility of them being promising hydrogen storage media is reduced. Hussain *et al.* employed the density functional theory (DFT) and reported that graphene under alkali and alkaline metal decoration behaves as a promising hydrogen storage candidate. ^{8,9}

Gao *et al.* successfully synthesized the monolayer, bilayer, and multilayer h-BN on Pt foils. ¹⁰ Later, Uchida *et al.* were also able to successfully grow a large-area multilayer h-BN for further utilization in gate-insulating materials and other practical purposes. ¹¹ The h-BN bilayer has been studied for its potential application in thermoelectric devices due to its superior electrical conductivity ¹² and for nano-electronic and opto-electronic devices by modulating the energy band gap by applying an external electric field, strain, doping, and so

Received: June 16, 2021 Accepted: August 12, 2021 Published: August 20, 2021





forth. 13-17 Extensive research on h-BN monolayer, graphitic carbon nitride, and boron carbide monolayer's potential reversible hydrogen storage system for mobile applications is in progress. 18-25 Panigrahi et al. reported an innovative coadsorption technique for hydrogen storage of lithiated carbon nitride (C_7N_6) . They reported that co-mixing of CH_4-H_2 and carbon nitride (C₇N₆) enhances the gravimetric density to 8.1 wt %, which is beyond the criteria set by US-DOE. 26 Chettri et al. reported the most probable H₂ adsorption site to be a hollow site and maximum H2 uptake capacity of the pristine h-BN monolayer to be 6.7 wt %, with an average adsorption energy of 0.13 eV/H₂.²⁷ Hu et al. performed a DFT-based comparative study for hydrogen storage properties of lithiumdecorated h-BN/graphene hybrid domains and reported the gravimetric density up to 8.7 wt %. 20 Recently, Banerjee et al. studied the 5.5-11.1% lithium fictionalized on the hydrogenated hexagonal boron nitride monolayer using DFT implemented in VASP. Lithium fictionalization enhances the gravimetric density (~6 wt %) and the average adsorption energy favorable for the adsorption/desorption process.²⁸ Hussain et al. highlighted the role of strain on the lithiumfictionalized graphene in enhancing the hydrogen storage capacity up to 12.12 wt %.²⁹ The application of an external electric field enhances the hydrogen storage ability of calciumdecorated silicene monolayer and bilayer.³ As reported earlier, the external electric field tunes the adsorption of the CO2 molecules on h-BN nanosheets.30 Also, ZnS monolayer and bilayer band gap tuning under the applied field has been successfully reported.³¹ As per our knowledge, the influence of the applied external electric field on hydrogen storage properties of the pristine h-BN bilayer has not been reported to date. Motivated by the abovementioned work, we present our DFT study on the h-BN bilayer for hydrogen storage applications in a field-free condition and in the presence of an external electric field incorporating van der Waals (vdW) potential.

COMPUTATIONAL DETAIL

All the calculations were performed using DFT implemented in the QuantumWise VNL-ATK code.³² We have employed a DFT-1/2^{33,34} method with generalized gradient approximation (GGA)-1/2 incorporating Grimme's DFT-D3 dispersion vdW correction to accurately describe the electron interaction energies in deriving the physical properties whereas GGA (LDA) fails. 35-40 GGA-1/2 is considered superior in predicting the energy band gap. In the DFT-1/2 methods, the electron-hole self-interaction energy is overcome by introducing atomic self-energy potential. The inclusion of the atomic self-energy potential to the DFT Hamiltonian helps to correctly predict the energy band gap of the semiconductor and the insulators. 33,34,41 A 3 \times 3 supercell of BN nanosheet is constructed with 18 (9 boron and 9 nitrogen) atoms in each layer, maintaining a boron-nitrogen ratio of 1:1. A vacuum of 25 Å is imposed along the Z-axis to avoid the interaction between the bilayers [see Figure 1a,b]. The PseudoDojo pseudopotential of boron, nitrogen, and hydrogen with a medium basis set is similar to the double ζ polarized basis set with a density mesh cut of 80 hartree.⁴² The conditions maintained for geometry optimization using the LBFGS algorithm⁴³ are (i) maximum force component less than 0.01 eV/Å on individual atoms, (ii) stress error tolerance of the order 10⁻⁴ eV/Å³, and (iii) the total energy changes below 10⁻⁵ eV. For all electronic calculations, we have used K-mesh

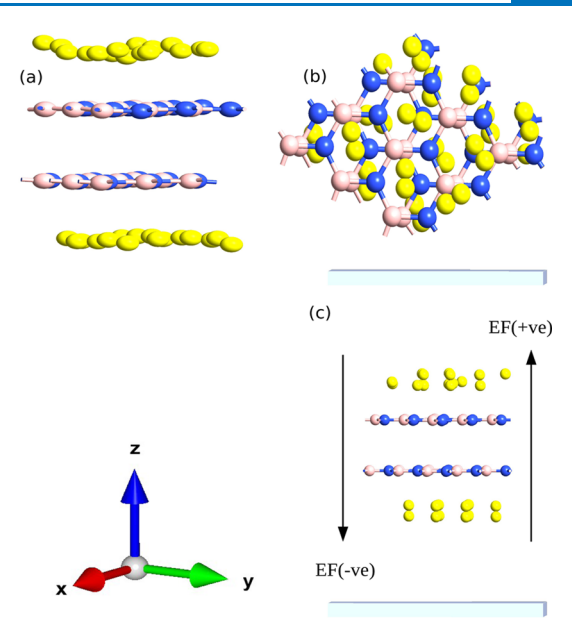


Figure 1. (a) Side view and (b) top view of the optimized structure of the hydrogen-adsorbed h-BN bilayer system and (c) H_2 h-BN bilayer under an external electric field (E_F) [direction of the applied field is given by E_F (+ve) and E_F (-ve)]. The brown color represents boron, blue represents nitrogen, and yellow represents hydrogen. The light blue box at the top and bottom are the electrodes.

of $24 \times 24 \times 1$ within the Monkhorst package.⁴⁴ We have considered two perpendicular directions normal to the h-BN bilayer system for applications of external electric field (i) along the +Z axis (positive field) and (ii) along the -Z axis (negative field) in the range ± 2 V/Å with an increment of 0.4 V/Å [see Figure 1c].

To understand the adsorption of $\rm H_2$ molecules on the h-BN bilayer, the quantitative value of binding energy ($E_{\rm BE}$) is obtained using ⁴⁵

$$E_{\rm BE} = E_{\rm BN} + nE_{\rm H_2} - E_{n\rm H_2 + BN} \tag{1}$$

Average adsorption energy ($E_{\rm ads}$ eV/ H_2) of adsorbed H_2 molecules on the h-BN bilayer system⁴⁵ is given by,

$$E_{\text{ads}} (\text{eV/H}_2) = \frac{E_{\text{BN}} + nE_{\text{H}_2} - E_{n\text{H}_2 + \text{BN}}}{n}$$
 (2)

where $E_{\rm BN}$, $E_{\rm H_2}$, and $E_{n{\rm H_2+BN}}$ are the total energies of the pristine h-BN bilayer, an isolated H₂ molecule, and H₂ molecules-adsorbed h-BN bilayer, respectively. The average adsorption energy is calculated in external field-free and external field conditions.

The hydrogen storage capacity is calculated in terms of gravimetric density using the following equation 27,45

$$H_2 \text{ (wt \%)} = \frac{nM_{H_2}}{(nM_{H_1} + M_{BN+Li})} \times 100$$
(3)

where $M_{\rm H_2}$ is the atomic mass of $\rm H_2$, $M_{\rm BN}$ is the atomic mass of the h-BN bilayer, and n denotes the number of adsorbed $\rm H_2$ molecules.

For the hydrogen storage system, the reversibility of H_2 adsorption \rightleftharpoons desorption is crucial. Therefore, the estimation of the desorption temperature is important to release the hydrogen molecules fully from the host materials. The

desorption temperature $T_{\rm D}$ (K) of the $\rm H_2$ molecules is computed using the following equation²⁷

$$T_{\rm D}(K) = \frac{E_{\rm ads}}{K_{\rm B}} \left(\frac{\Delta S}{R} - \ln P\right)^{-1} \tag{4}$$

where $E_{\rm ads}$, R = 8.31 J K⁻¹ mol⁻¹, $K_{\rm B} = 1.38 \times 10^{-23}$ J K⁻¹, $\Delta S = 75.44$ J K⁻¹ mol⁻¹, and P indicate average adsorption energy, gas constant, Boltzmann constant, and change in the H₂ entropy from gas to the liquid phase at the equilibrium pressure P = 1 atm, respectively.

The recovery rate is calculated using the following equation

$$\tau = \nu_0^{-1} \,\mathrm{e}^{-E_{\rm ads}/K_{\rm B}T} \tag{5}$$

where ν_0 is the attempted frequency (10^{12} s^{-1}) and E_{ads} is the adsorption energy. We have calculated the recovery rate considering temperature (T) = 300 K.

RESULT AND DISCUSSION

In this section, the structural parameters and electronic properties of the pristine hexagonal boron nitride bilayer

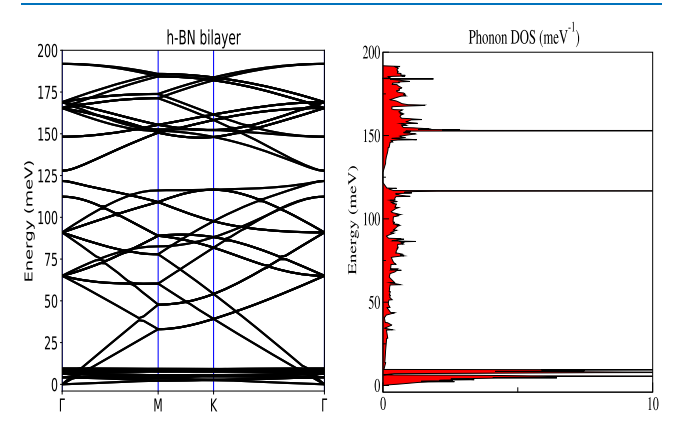


Figure 2. Phonon band structure and phonon DOS for the h-BN bilayer system. The positive phonon bands starting from 0 meV resembles the thermodynamical stability of the h-BN bilayer.

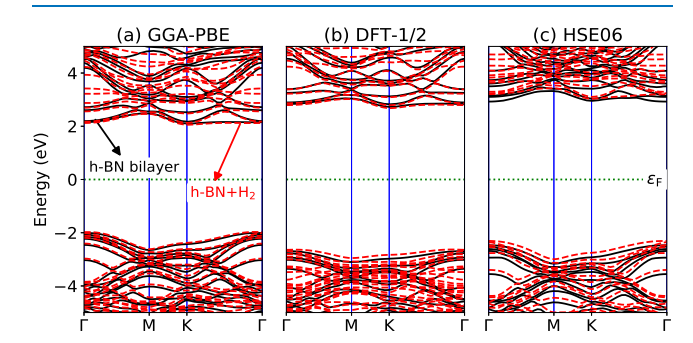


Figure 3. Band structures of the pristine and hydrogen-adsorbed hBN bilayer in the absence of electric field calculated from (a) GGA-PBE, (b) DFT-1/2, and (c) HSE06 (black solid line denotes h-BN without $\rm H_2$ and the red dotted line represents h-BN with $\rm H_2$). The Fermi level is denoted by a dotted horizontal line at 0 eV.

stacked in AB configuration have been discussed. The optimized interlayer distance is 3.34 Å. The bond length between B–N is found to be 1.45 Å. The thermodynamic stability of the bilayer h-BN is tested by calculating the phonon dispersion [Figure 2]. The positive phonon bands (phonon frequencies) validate the thermodynamic stability of the h-BN

bilayer. The application of vdW potential plays a major role in maintaining the stability of bilayer systems. Zhang et al. reported the enhanced stability of GaSe/CN and Ga₂SSe/CN heterostructures by considering vdW interaction. 46 Li et al. have also reported that the carbon nanomaterial acts as an effective anchor in Li-S ions batteries employing vdW. 47 He et al. have reported that HSE is an effective tool in opening the electronic band gap of bilayer In₂SeS/g-C₃N₄ heterojunction and metal organic framework materials. 48,49 As the previously reported band gap of the h-BN system lies within a range of 4.0-5.8 eV, 14,15,50 these data can be used for future references and comparison. The calculated band structures of pristine and H₂ adsorbed h-BN bilayer within field-free condition from GGA, DFT-1/2, and HSE06 is presented in Figure 3a-c. In our band structure calculation from GGA-PBE, 51 DFT-1/ 2,33,34 and HSE0652 approaches, we have found that the h-BN bilayer is a large band gap semiconductor with energy band gap values of 4.11, 5.40, and 5.39 eV, respectively. The band gap energy of the h-BN bilayer predicted using hybrid functional and DFT-1/2 method is of the same order. Moreover, the advantage of using DFT-1/2 is that it falls within the semilocal approach; hence, the calculation converge in feasible time, saving all the computational expenses. Observation of band structure diagram and density of states (DOS) plot revealed that the B 2p states populated the conduction band and N 2p states populated the valence band, respectively.

Adsorption of H₂ on the Pristine h-BN Bilayer in an External Field-Free Condition ($E_F = 0.0 \text{ V/Å}$). This section is dedicated to the discussion about the adsorption of H₂ molecules on the pristine hexagonal boron nitride bilayer system. As observed from the optimized atomic structure, H₂ molecules tend to reside on the hollow hexagonal site of the h-BN bilayer. Similar observation about the hollow hexagonal site being the probable site for hydrogen adsorption has been reported for graphene, h-BN nanosheet, and so forth.²⁷ We have not followed a fabrication process to build the reservoir of H₂ molecules into the h-BN bilayer, as there is no risk of clusterization of H2 molecules at the surface or migration on the surface of host materials in the absence of decoration or doping with other atoms. Initially, all H2 molecules were oriented parallel to the plane of the h-BN bilayer, and under optimization, some of the H₂ molecules tilted due to H₂-H₂ self-interaction. With the introduction of hydrogen molecules, interlayer spacing increased to 3.67 Å. The optimized average vertical distance of the H₂ molecules on the top and bottom layer is between 2.78 and 3.1 Å. The free H₂ molecule has a bond length of 0.74 Å. Under adsorption, H-H bond length varies between 0.74 and 0.75 Å and remains in molecular form.⁵³ The effect of hydrogen molecule adsorption on the electronic band structure of the h-BN bilayer under the field $E_{\rm F}$ = 0.0 V/Å has been presented in Figure 3a-c. The calculated energy band gap values of the H₂-adsorbed h-BN bilayer in the field-free condition are found to be 4.08 eV (GGA-PBE), 5.38 eV (DFT-1/2), and 5.33 eV (HSE06), which are lower than the band gap values of the pristine system. The partial density of states (PDOS) of the hydrogen molecule-adsorbed h-BN bilayer in terms of B 2pz, N 2pz and H 1s orbital contribution denoted by red, green, and blue stacked color state is presented in Figure 4a. As evident from the DOS plot, the valence and conduction band is dominated by the N 2pz and B 2pz orbital, respectively (see Figure 4a). H 1s orbital contribution is observed beyond the ± 2.5 eV energy range (see Figure 4a).

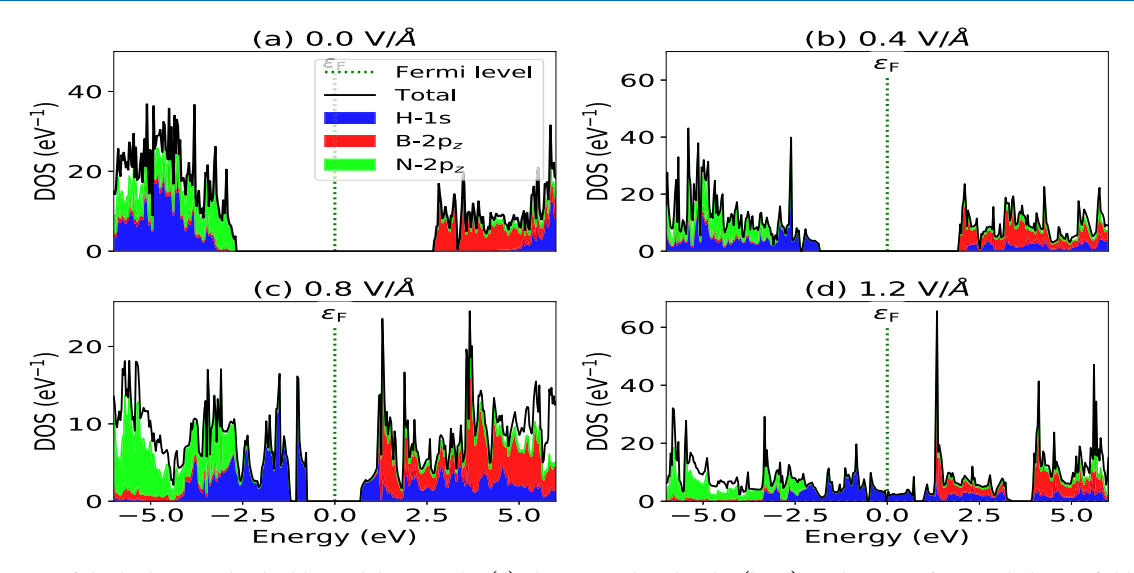


Figure 4. PDOS of the hydrogen-adsorbed h-BN bilayer in the (a) absence and under the (b-d) application of external electric field. The Fermi level is denoted by a dotted vertical line at 0 eV.

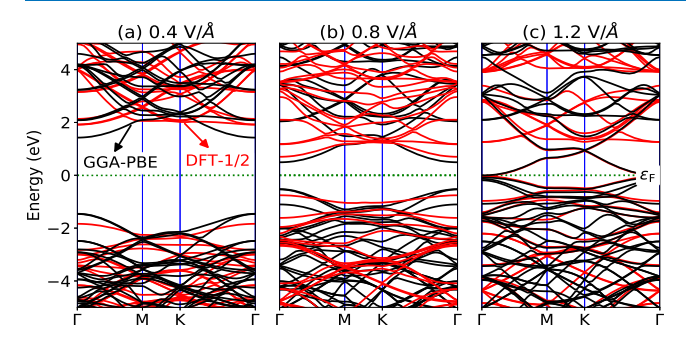


Figure 5. Band structures of the hydrogen-adsorbed h-BN bilayer applying the electric field in the positive direction within DFT-1/2: (a) $E_{\rm F} = 0.4$ V/Å, (b) $E_{\rm F} = 0.8$ V/Å, and (c) $E_{\rm F} = 1.2$ V/Å. The Fermi level is denoted by a dotted horizontal line at 0 eV.

Table 1. Calculated Energy Band gap $(E_{\rm g})$ from the DFT-1/2 Method, Average Adsorption Energies $(E_{\rm ads})$, the Percent Change of the Average Adsorption Energy $(\Delta_{\rm ads})$ Induced by External Electric Field, Desorption Temperature $(T_{\rm D})$, and Recovery Rate (τ) of the Hydrogen-Adsorbed Hexagonal Boron Nitride Bilayer System under the Influence of External Electric Field $(E_{\rm F})$ Incorporating the Grimme's DFT-D3 Dispersion Correction

$E_{ m F} m (V/\AA)$	$\frac{E_{\rm g}}{({ m eV})}$	$\frac{E_{\mathrm{ads}}}{(\mathrm{eV/H_2})}$	$egin{pmatrix} \Delta_{ m ads} \ (\%) \end{pmatrix}$	wt %	$T_{\mathrm{D}}\left(\mathrm{K}\right)$	recovery rate (τ) (s)
-2.0	0.00	0.846	279.3	6.7	668.98	179.66 s
-1.6	0.00	0.672	201.3	6.7	531.38	0.210 s
-1.2	0.00	0.560	151.1	6.7	442.44	0.002 s
-0.8	1.450	0.499	123.7	6.7	394.49	0.0002 s
-0.4	3.750	0.465	108.5	6.7	367.59	$68.03 \ \mu s$
0.0	5.382	0.223		6.7	176.76	5.80 ns
0.4	3.756	0.465	108.5	6.7	367.86	68.92 μs
0.8	1.457	0.500	124.2	6.7	395.06	0.0002 s
1.2	0.00	0.560	151.1	6.7	442.65	0.002 s
1.6	0.00	0.671	200.8	6.7	530.40	0.200 s
2.0	0.00	0.845	278.9	6.7	667.97	171.00 s

Furthermore, there is no overlapping of electron distribution between the h-BN bilayer and H_2 molecules, thus validating the holding mechanism of H_2 molecules *via* weak vdW

interactions. Total energies of the h-BN bilayer and $\rm H_2$ molecule-adsorbed bilayer are calculated in a field-free condition. In an external field-free condition, the calculated weight percentage of $\rm H_2$ molecules and average adsorption energy of $\rm H_2$ molecules on the h-BN bilayer are 6.7 wt % and 0.223 eV/ $\rm H_2$, respectively. The calculated desorption temperature, in this case, is ~176 K. The hydrogen storage capacity and average adsorption energy lie within the benchmark set by US-DOE, 45,54 whereas the desorption temperature is slightly less than the room temperature. The desorption temperature can be further increased by the introduction of an external electric field ($E_{\rm F}$).

Effect of External Electric Field on H₂ Adsorption on the h-BN Bilayer. In this section, we will discuss the hydrogen storage ability of the h-BN bilayer system in the presence of the external electric field. The external electric field is introduced normal to the hydrogen molecule-adsorbed h-BN bilayer in the range [-2.0, 2.0 V/Å] with an increment of 0.4 V/Å in two directions, that is, bottom to the top layer (positive) and top to the bottom layer (negative) of the h-BN bilayer (see Figure 1c). The calculated band structure of the hydrogen molecule-adsorbed h-BN bilayer system under the applied electric field (0.4 to 1.2 eV/Å) is presented in Figure 5a-c. We first investigated the effect of different external field intensities on the bond lengths of adsorbed H₂ molecules, interlayer h-BN bilayer distance, and the adsorbed H2 molecule distance from the h-BN top and bottom layer plane. The hydrogen molecules aligned perpendicular to the plane of the h-BN bilayer when optimized under the external field at different field strength values. We observed an elongation in the bond length up to 0.78 Å compared to the free H₂ molecule bond length of 0.74 Å. The h-BN bilayer distance was increased by ~ 0.33 Å with the increase in the applied electric field strength. Because the effect of negative and the positive electric field on the hydrogen-adsorbed h-BN bilayer was symmetric; we have presented the data for the positive field only. The PDOS and band structure have been presented in Figures 4b-d and 5a-c, respectively, to elucidate the electronic properties of the H₂ molecule-adsorbed h-BN bilayer in the presence of the external electric field. The quantitative analysis of variation of the energy band gap

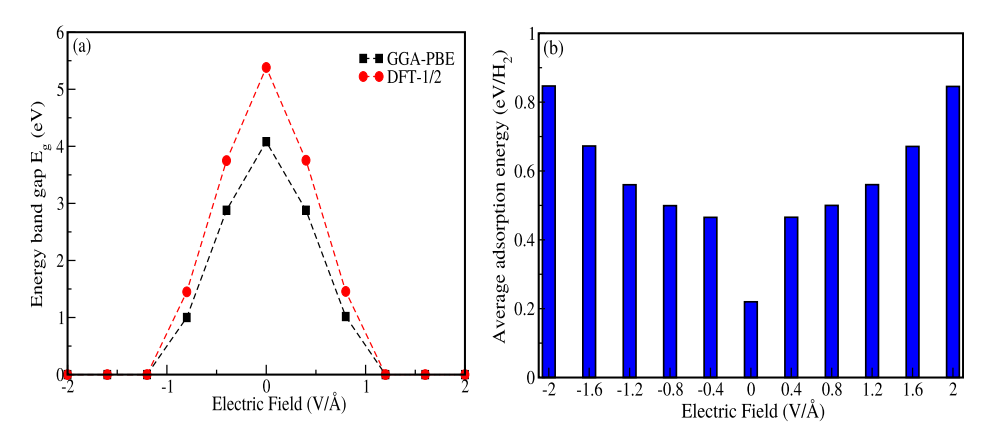


Figure 6. (a) Variation of energy band gap with external electric field. The energy band gap is obtained using GGA-PBE (black color) and DFT-1/2 (red color) method employing Grimme's DFT-D3 dispersion correction. (b) Variation of average adsorption energy with respect to an external electric field.

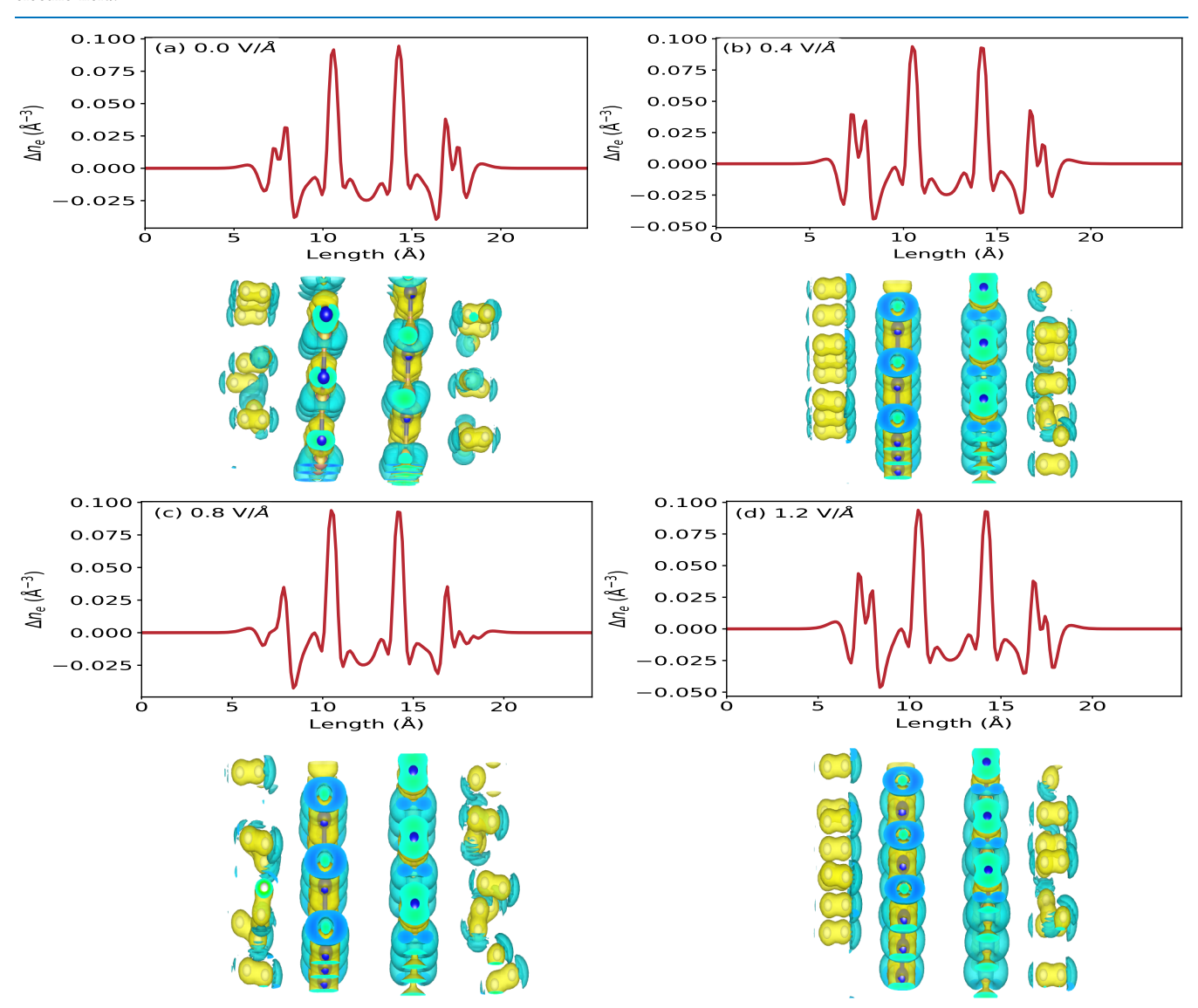


Figure 7. Electron density difference with an isovalue of 0.02 Å^{-3} and the planar average electron density difference plot of the optimized (a) hydrogen-adsorbed h-BN bilayer and (b-d) hydrogen-adsorbed h-BN bilayer under external field of strength 0.4-1.2 V/Å. The planar average electron density difference (labeled as a-d) and 3D electron density difference plots (right below a-d) are arranged in the top and bottom manner, respectively.

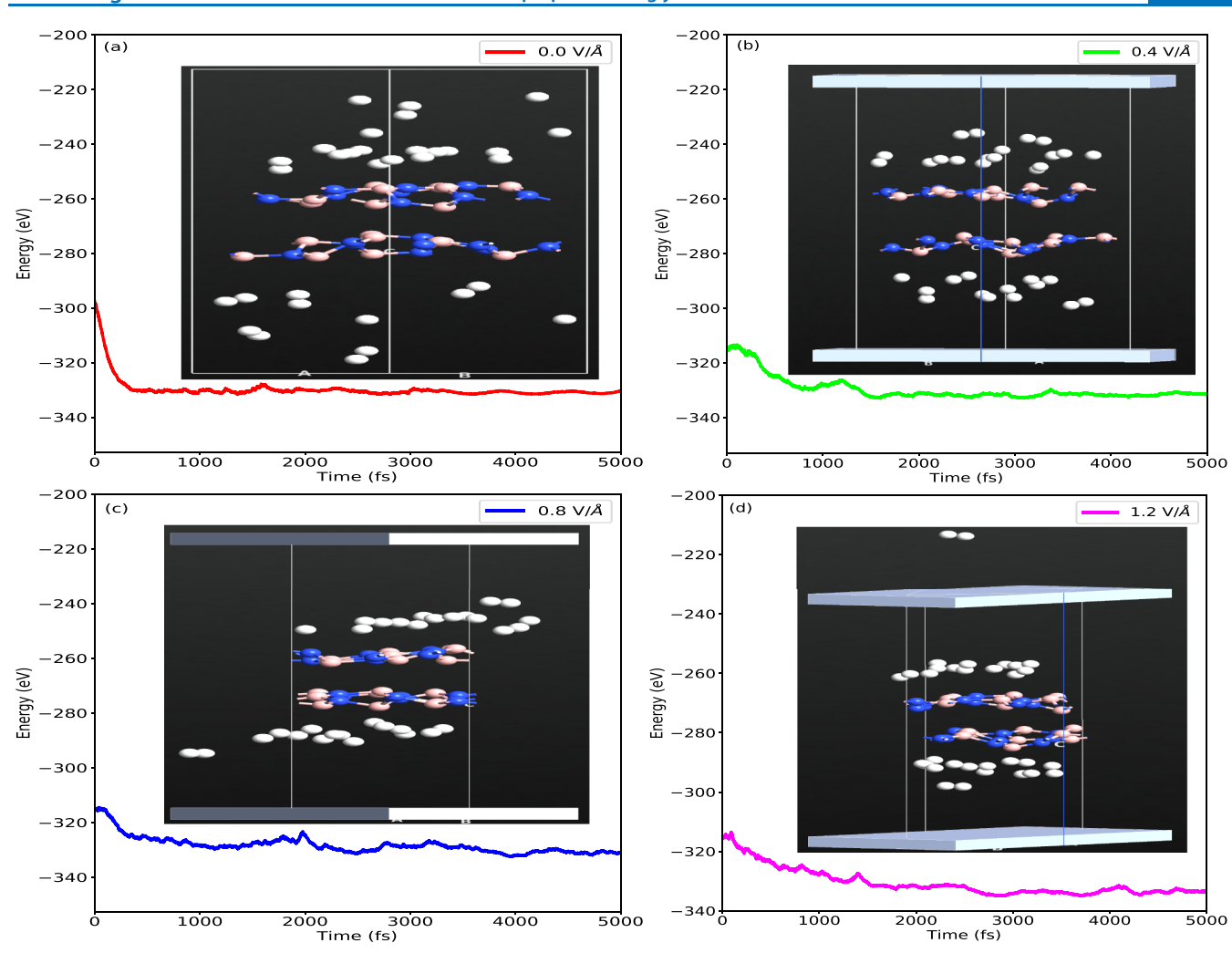


Figure 8. MD plots for the hydrogen-adsorbed h-BN bilayer system with and without the application of positive $[E_{\rm F}\ (+{\rm ve})]$ external electric field at temperature $(T) = 300\ {\rm K.}$ (a) $E_{\rm F} = 0.0\ {\rm V/Å}$, (b) $E_{\rm F} = 0.4\ {\rm V/Å}$, (c) $E_{\rm F} = 0.8\ {\rm V/Å}$, and (d) $E_{\rm F} = 1.2\ {\rm V/Å}$. (The hydrogen-adsorbed structure after the MD simulation is shown in the inset.)

obtained from GGA-PBE with Grimme's DFT-D3 and DFT-1/2 method versus positive and negative external fields is summarized in Table 1.

The effect of different electric field intensities on the electronic properties of the hydrogen-adsorbed h-BN bilayer system can be analyzed from Figures 4 and 5. A substantial change in the band gap has been observed with the variation of the applied electric field (see Figure 6a). In the absence of the external field, the H 1s orbital contribution is least dominant around the valence and the conduction band, whereas upon substantial increment in the strength of the external electric field, the H 1s orbital contribution becomes dominant in the valence and conduction band region, as evident from Figure 4a-d. The system becomes fully metallic beyond the electric field strength of $\pm 1.2 \text{ V/Å}$. The effect of the negative external electric field on the electronic properties is also symmetric with the positive external field. The variation in the energy band gap of H₂-adsorbed h-BN bilayer system under an applied external electric field at the same intensity but in the opposite direction is less than 0.006-0.007 eV.

We have calculated the desorption temperature $(T_{\rm D})$ for H_2 molecules presented in Table 1. From eq 4, it is evident that desorption temperature is dependent on the average adsorption energy. In our study, the external electric field

enhances the average adsorption energy and thus increases the desorption temperature (T_D) (see Table 1). The desorption temperature under different external electric fields lies in the range 176-668 K with average adsorption energy in the range 0.223-0.846 eV/H₂. Therefore, the external electric field can effectively stabilize the h-BN bilayer structure with an average adsorption energy of 0.223-0.846 eV/H₂ and desorption at temperature 176-668 K, which is near ambient temperatures. The external positive and negative electric fields have a similar effect on the energy band gap (E_g) and the average adsorption energy (E_{ads}) (see Table 1). The average adsorption energy has been significantly increased upon the introduction of electric field (see Figure 6b). The percent change in average adsorption energy (Δ_{ads}) with respect to the applied external electric field is shown in Table 1. With the increase in electric field strength, the adsorption energy also increases. Also, the electronic property of the host material has been tuned by the application of an external electric field. With the increase in external field strength, bands are shifted near the Fermi level, and thus, it reduces the energy band gap.

To have a better understanding of the charge transfer mechanism between the h-BN layer and the hydrogen molecules, electron density difference and planar average electron difference are plotted in Figure 7. The electron density difference distribution plot indicates the ioniccovalent type bonding characteristics between B (brown)-N (blue) in a h-BN bilayer system, as the charges are mostly localized on N-atom, and feeble distribution between the B-N bond is shown in Figure 7a-d. As observed from the electron density difference plot, most of the electrons are localized around the nitrogen atom (blue). Also, the charge transfer between the h-BN layer is absent. The light blue and yellow lobes around the respective atoms resemble the electron depletion and accumulation, respectively. 48,55,56 From the planar average electron density difference plots under the application of different external electric fields, a charge distribution between B and N atoms in the respective h-BN layers is observed, as shown in Figure 7a-d. The nitrogen atoms became more negative (covered with yellow lobe), and boron atoms (covered with light blue lobe) become more positive (see Figure 7). Similarly, charge distribution in the hydrogen molecules can be seen from the three-dimensional (3D) plots as well as the average planar plots. The peaks and valleys between the 5-10 and 16-20 Å resemble the electron accumulation and depletion between the respective h-BN surface and the H₂ molecules.

We have performed an ab initio molecular dynamics (MD) simulation using the Nose-Hoover algorithm⁵⁷ to test the dynamic and structural stability of the H2 molecule-adsorbed h-BN bilayer system under the external electric field in positive directions at room temperature. The total energy versus time steps plot at a finite temperature of 300 K is shown in Figure 8b-d, which is under the influence of the external electric field in positive directions. We have performed the MD simulation of the hydrogen-adsorbed h-BN bilayer system for 5000 fs with a 1 fs time step. The final structure of the hydrogen-adsorbed system after 5000 fs is shown in the respective figures. A buckling in the h-BN bilayer is observed after the 5000 dynamic simulation, and 5 H₂ molecules moved away in the case of 0.8 V/Å and 1 H₂ in the case of 1.2 V/Å. In contrast, other hydrogen molecules remain in the vicinity of the h-BN bilayer. As the h-BN system maintains its signature even after 5000 fs, it can be utilized for the reversible hydrogen molecule storage.

CONCLUSIONS

In this study, DFT calculations have been performed to study the effect of the external electric field on the hydrogen storage properties of the h-BN bilayer. The thermodynamic stability of the H₂-adsorbed h-BN bilayer system was studied using ab initio MD using the Nose-Hoover algorithm, as programed in QuantumWise VNL-ATK. The electronic properties of the hydrogen molecule-adsorbed h-BN bilayer system is modified by the application of the external electric field. The energy band gap has been tuned from 5.382 eV ($E_F = 0.0 \text{ V/Å}$) to 0.0 eV ($E_{\rm F}$ = 1.2 V/Å). Beyond the applied electric field of 1.2 (-1.2) V/Å, the H₂ adsorbed system exhibits metallic behavior with a diminished energy band gap. In the external field-free condition ($E_F = 0.0 \text{ V/Å}$), the h-BN bilayer with 16 H₂adsorbed molecules have a gravimetric density of 6.7 wt % and an average adsorption energy of 0.223 eV/H₂. The corresponding desorption temperature is ~176 K. On the other hand, the application of the external electric field (-2.0)to 2.0) V/Å enhances the overall hydrogen adsorption ability of the h-BN bilayer. Average adsorption energy ranges between 0.223 and 0.846 eV/H₂, and the desorption temperature ranges from 176 to 668 K. Our study revealed that the binding

strength and the desorption temperature of the $\rm H_2$ molecules are increased under the application of external electric fields due to the high value of adsorption energy. Thus h-BN bilayer system can be a potential $\rm H_2$ storage material under applied electric field.

AUTHOR INFORMATION

Corresponding Author

Dibya Prakash Rai — Physical Sciences Research Center (PSRC), Department of Physics, Pachhunga University College, Mizoram University, Aizawl 796001, India; orcid.org/0000-0002-3803-8923; Email: dibya@pucollege.edu.in

Authors

Bhanu Chettri – Department of Physics, North-Eastern Hill University, Shillong, Meghalaya 793022, India; Physical Sciences Research Center (PSRC), Department of Physics, Pachhunga University College, Mizoram University, Aizawl 796001, India

Prasanta Kumar Patra — Department of Physics, North-Eastern Hill University, Shillong, Meghalaya 793022, India Sunita Srivastava — Department of Physics, Guru Jambheshwar University of Science & Technology, Hisar 125001 Haryana, India; Department of Physics, Panjab

Amel Laref – Department of Physics and Astronomy, College of Science, King Saud University, Riyadh 11451, Saudi

Complete contact information is available at: https://pubs.acs.org/10.1021/acsomega.1c03154

University, Chandigarh 160014, India

Notes

The authors declare no competing financial interest.

ACKNOWLEDGMENTS

D.P.R. acknowledges support from the Department of Science and Technology SERB (CRG DST-SERB, Govt. of India, New Delhi) *via* sanction no. CRG/2018/000009 (Ver-1). A.L. acknowledges support from the "Research Center of the Female Scientific and Medical Colleges", Deanship of Scientific Research, King Saud University, Saudi Arabia.

REFERENCES

- (1) Naqvi, S. R.; Hussain, T.; Luo, W.; Ahuja, R. Metallized siligraphene nanosheets (SiC7) as high capacity hydrogen storage materials. *Nano Res.* **2018**, *11*, 3802–3813.
- (2) Hussain, T.; Islam, M. S.; Rao, G. S.; Panigrahi, P.; Gupta, D.; Ahuja, R. Hydrogen storage properties of light metal adatoms (Li, Na) decorated fluorographene monolayer. *Nanotechnology* **2015**, *26*, 275401.
- (3) Song, E. H.; Yoo, S. H.; Kim, J. J.; Lai, S. W.; Jiang, Q.; Cho, S. O. External electric field induced hydrogen storage/release on calcium-decorated single-layer and bilayer silicene. *Phys. Chem. Chem. Phys.* **2014**, *16*, 23985–23992.
- (4) Zheng, N.; Yang, S.; Xu, H.; Lan, Z.; Wang, Z.; Gu, H. A DFT study of the enhanced hydrogen storage performance of the Lidecorated graphene nanoribbons. *Vacuum* **2020**, *171*, 109011.
- (5) Wang, J.; Du, Y.; Sun, L. Ca-decorated novel boron sheet: A potential hydrogen storage medium. *Int. J. Hydrogen Energy* **2016**, *41*, 5276–5283.
- (6) Rai, D. P.; Vu, T. V.; Laref, A.; Ghimire, M. P.; Patra, P. K.; Srivastava, S. Electronic and optical properties of 2D monolayer (ML)

- MoS2 with vacancy defect at S sites. Nano-Struct. Nano-Objects 2020, 21, 100404.
- (7) Rai, D. P.; Vu, T. V.; Laref, A.; Joshi, H.; Patra, P. K. Promising optoelectronic response of 2D monolayer MoS2: A first principles study. *Chem. Phys.* **2020**, *538*, 110824.
- (8) Hussain, T.; Pathak, B.; Adit Maark, T.; Moyses Araujo, C.; Scheicher, R. H.; Ahuja, R. Ab initio study of lithium-doped graphane for hydrogen storage. *Europhys. Lett.* **2011**, *96*, 27013.
- (9) Hussain, T.; Pathak, B.; Ramzan, M.; Maark, T. A.; Ahuja, R. Calcium doped graphane as a hydrogen storage material. *Appl. Phys. Lett.* **2012**, *100*, 183902.
- (10) Gao, Y.; Ren, W.; Ma, T.; Liu, Z.; Zhang, Y.; Liu, W. B.; Ma, L. P.; Ma, X.; Cheng, H. M. Repeated and controlled growth of monolayer, bilayer and few-layer hexagonal boron nitride on Pt foils. *ACS Nano* **2013**, *7*, 5199–5206.
- (11) Uchida, Y.; Nakandakari, S.; Kawahara, K.; Yamasaki, S.; Mitsuhara, M.; Ago, H. Controlled Growth of Large-Area Uniform Multilayer Hexagonal Boron Nitride as an Effective 2D Substrate. *ACS Nano* **2018**, *12*, 6236–6244.
- (12) Wang, C.; Guo, J.; Dong, L.; Aiyiti, A.; Xu, X.; Li, B. Superior thermal conductivity in suspended bilayer hexagonal boron nitride. *Sci. Rep.* **2016**, *6*, 25334.
- (13) Abergel, D. S.; Mucha-Kruczyński, M. Infrared absorption of closely aligned heterostructures of monolayer and bilayer graphene with hexagonal boron nitride. *Phys. Rev. B: Condens. Matter Mater. Phys.* **2015**, 92, 115430.
- (14) Amiri, M.; Beheshtian, J.; Shayeganfar, F.; Faghihnasiri, M.; Shahsavari, R.; Ramazani, A. Electro-optical properties of monolayer and bilayer pentagonal BN: First principles study. *Nanomaterials* **2020**, *10*, 440.
- (15) Chettri, B.; Patra, P. K.; Lalmuanchhana; Lalhriatzuala; Verma, S.; Rao, B. K.; Verma, M. L.; Thakur, V.; Kumar, N.; Hieu, N. N.; Rai, D. P. Induced magnetic states upon electron—hole injection at B and N sites of hexagonal boron nitride bilayer: A density functional theory study. *Int. J. Quantum Chem.* **2021**, *121*, No. e26680.
- (16) Laturia, A.; Van de Put, M. L.; Vandenberghe, W. G. Dielectric properties of hexagonal boron nitride and transition metal dichalcogenides: from monolayer to bulk. *npj 2D Mater. Appl.* **2018**, *2*, 6.
- (17) Ansari, R.; Faghihnasiri, M.; Malakpour, S.; Sahmani, S. Effect of electric field on the mechanical properties of bilayer boron nitride with AB stacking order: An ab initio study. *Superlattices Microstruct.* **2015**, 83, 498–506.
- (18) Hussain, T.; Searles, D. J.; Takahashi, K. Reversible Hydrogen Uptake by BN and BC3 Monolayers Functionalized with Small Fe Clusters: A Route to Effective Energy Storage. *J. Phys. Chem. A* **2016**, *120*, 2009–2013.
- (19) Alhameedi, K.; Hussain, T.; Bae, H.; Jayatilaka, D.; Lee, H.; Karton, A. Reversible hydrogen storage properties of defect-engineered C4N nanosheets under ambient conditions. *Carbon* **2019**, *152*, 344–353.
- (20) Hu, Z. Y.; Shao, X.; Wang, D.; Liu, L. M.; Johnson, J. K. A first-principles study of lithium-decorated hybrid boron nitride and graphene domains for hydrogen storage. *J. Chem. Phys.* **2014**, *141*, 084711.
- (21) Hu, S.; Yong, Y.; Zhao, Z.; Gao, R.; Zhou, Q.; Kuang, Y. C7N6 monolayer as high capacity and reversible hydrogen storage media: A DFT study. *Int. J. Hydrogen Energy* **2021**, *46*, 21994–22003.
- (22) Li, Y.; Hussain, T.; De Sarkar, A.; Ahuja, R. Hydrogen storage in polylithiated BC3 monolayer sheet. *Solid State Commun.* **2013**, *170*, 39–43.
- (23) Li, L.; Zhang, H.; Cheng, X. The high hydrogen storage capacities of Li-decorated borophene. *Comput. Mater. Sci.* **2017**, *137*, 119–124.
- (24) Mananghaya, M. R. A simulation of hydrogen adsorption/desorption in metal-functionalized BN nanotube. *Mater. Chem. Phys.* **2020**, 240, 122159.
- (25) Naqvi, S. R.; Hussain, T.; Panigrahi, P.; Luo, W.; Ahuja, R. Manipulating energy storage characteristics of ultrathin boron carbide

- monolayer under varied scandium doping. RSC Adv. 2017, 7, 8598–8605.
- (26) Panigrahi, P.; Acharya, D.; Selvi, S. R.; Ahuja, R.; Hussain, T. Enhancing energy storage efficiency of lithiated carbon nitride (C7N6) monolayers under co-adsorption of H2 and CH4. *Int. J. Hydrogen Energy* **2021**, *46*, 19988–19997.
- (27) Chettri, B.; Patra, P. K.; Hieu, N. N.; Rai, D. P. Hexagonal boron nitride (h-BN) nanosheet as a potential hydrogen adsorption material: A density functional theory (DFT) study. *Surf. Interfaces* **2021**, *24*, 101043.
- (28) Banerjee, P.; Pathak, B.; Ahuja, R.; Das, G. P. First principles design of Li functionalized hydrogenated h-BN nanosheet for hydrogen storage. *Int. J. Hydrogen Energy* **2016**, *41*, 14437–14446.
- (29) Hussain, T.; De Sarkar, A.; Ahuja, R. Strain induced lithium functionalized graphane as a high capacity hydrogen storage material. *Appl. Phys. Lett.* **2012**, *101*, 103907.
- (30) Sun, Q.; Li, Z.; Searles, D. J.; Chen, Y.; Lu, G.; Du, A. Charge-Controlled Switchable CO 2 Capture on Boron Nitride Nanomaterials. *J. Am. Chem. Soc.* **2013**, *135*, 8246–8253.
- (31) Rai, D. P.; Kaur, S.; Srivastava, S. Band gap modulation of mono and bi-layer hexagonal ZnS under transverse electric field and bi-axial strain: A first principles study. *Phys. B* **2018**, 531, 90–94.
- (32) Smidstrup, S.; et al. QuantumATK: An integrated platform of electronic and atomic-scale modelling tools. *J. Phys.: Condens. Matter* **2020**, 32, 015901.
- (33) Ferreira, L. G.; Marques, M.; Teles, L. K. Approximation to density functional theory for the calculation of band gaps of semiconductors. *Phys. Rev. B: Condens. Matter Mater. Phys.* **2008**, 78, 125116.
- (34) Ferreira, L. G.; Marques, M.; Teles, L. K. Slater half-occupation technique revisited: The LDA-1/2 and GGA-1/2 approaches for atomic ionization energies and band gaps in semiconductors. *AIP Adv.* **2011**, *1*, 032119.
- (35) Lee, K.; Murray, É. D.; Kong, L.; Lundqvist, B. I.; Langreth, D. C. Higher-accuracy van der Waals density functional. *Phys. Rev. B: Condens. Matter Mater. Phys.* **2010**, 82, No. 081101(R).
- (36) Hussain, T.; Chakraborty, S.; De Sarkar, A.; Johansson, B.; Ahuja, R. Enhancement of energy storage capacity of Mg functionalized silicene and silicane under external strain. *Appl. Phys. Lett.* **2014**, *105*, 123903.
- (37) Hussain, T.; Hankel, M.; Searles, D. J. Graphenylene Monolayers Doped with Alkali or Alkaline Earth Metals: Promising Materials for Clean Energy Storage. *J. Phys. Chem. C* **2017**, *121*, 14393–14400.
- (38) Panigrahi, P.; Kumar, A.; Karton, A.; Ahuja, R.; Hussain, T. Remarkable improvement in hydrogen storage capacities of two-dimensional carbon nitride (g-C3N4) nanosheets under selected transition metal doping. *Int. J. Hydrogen Energy* **2020**, *45*, 3035–3045.
- (39) Buimaga-Iarinca, L.; Morari, C. Adsorption of small aromatic molecules on gold: a DFT localized basis set study including van der Waals effects. *Theor. Chem. Acc.* **2014**, *133*, 1502.
- (40) Grimme, S.; Antony, J.; Ehrlich, S.; Krieg, H. A consistent and accurate ab initio parametrization of density functional dispersion correction (DFT-D) for the 94 elements H-Pu. *J. Chem. Phys.* **2010**, 132, 154104.
- (41) Yuan, J. H.; Chen, Q.; Fonseca, L. R.; Xu, M.; Xue, K. H.; Miao, X. S. GGA-1/2 self-energy correction for accurate band structure calculations: The case of resistive switching oxides. *J. Phys. Commun.* **2018**, *2*, 105005.
- (42) van Setten, M. J.; Giantomassi, M.; Bousquet, E.; Verstraete, M. J.; Hamann, D. R.; Gonze, X.; Rignanese, G.-M. The PseudoDojo: Training and grading a 85 element optimized norm-conserving pseudopotential table. *Comput. Phys. Commun.* **2018**, 226, 39–54.
- (43) Liu, D. C.; Nocedal, J. On the limited memory BFGS method for large scale optimization. *Math. Program.* **1989**, *45*, 503–528.
- (44) Monkhorst, H. J.; Pack, J. D. Special points for Brillouin-zone integrations. *Phys. Rev. B: Solid State* **1976**, *13*, 5188–5192.

- (45) Varunaa, R.; Ravindran, P. Potential hydrogen storage materials from metal decorated 2D-C2N: An: ab initio study. *Phys. Chem. Chem. Phys.* **2019**, *21*, 25311–25322.
- (46) Zhang, W. X.; Yin, Y.; He, C. Spontaneous Enhanced Visible-Light-Driven Photocatalytic Water Splitting on Novel Type-II GaSe/CN and Ga2SSe/CN vdW Heterostructures. *J. Phys. Chem. Lett.* **2021**, *12*, 5064–5075.
- (47) Li, T.; He, C.; Zhang, W. Rational design of porous carbon allotropes as anchoring materials for lithium sulfur batteries. *J. Energy Chem.* **2021**, *52*, 121–129.
- (48) He, C.; Han, F. S.; Zhang, J. H.; Zhang, W. X. The In2SeS/g-C3N4heterostructure: A new two-dimensional material for photocatalytic water splitting. *J. Mater. Chem. C* **2020**, *8*, 6923–6930.
- (49) Li, T.; He, C.; Zhang, W. Two-dimensional porous transition metal organic framework materials with strongly anchoring ability as lithium-sulfur cathode. *Energy Storage Mater.* **2020**, *25*, 866–875.
- (50) Chettri, B.; Patra, P. K.; Vu, T. V.; Nguyen, C. Q.; Lalrinkima; Yaya, A.; Obodo, K. O.; Tran, N. T. T.; Laref, A.; Rai, D. P. Induced ferromagnetism in bilayer hexagonal Boron Nitride (h-BN) on vacancy defects at B and N sites. *Phys. E* **2021**, *126*, 114436.
- (51) Perdew, J. P.; Burke, K.; Ernzerhof, M. Generalized gradient approximation made simple. *Phys. Rev. Lett.* **1996**, *77*, 3865–3868.
- (52) Heyd, J.; Scuseria, G. E.; Ernzerhof, M. Hybrid functionals based on a screened Coulomb potential. *J. Chem. Phys.* **2003**, *118*, 8207.
- (53) López-Corral, I.; Germán, E.; Juan, A.; Volpe, M. A.; Brizuela, G. P. DFT study of hydrogen adsorption on palladium decorated graphene. *J. Phys. Chem. C* **2011**, *115*, 4315–4323.
- (54) Schlapbach, L.; Züttel, A. Materials for Sustainable Energy: A Collection of Peer-Reviewed Research and Review Articles from Nature Publishing Group; World Scientific Publishing Co., 2010; pp 265–270.
- (55) Zhang, W. X.; Yin, Y.; He, C. Lowering the Schottky barrier height of G/WSSe van der Waals heterostructures by changing the interlayer coupling and applying external biaxial strain. *Phys. Chem. Chem. Phys.* **2020**, 22, 26231–26240.
- (56) He, C.; Zhang, J. H.; Zhang, W. X.; Li, T. T. Type-II InSe/g-C3N4 Heterostructure as a High-Efficiency Oxygen Evolution Reaction Catalyst for Photoelectrochemical Water Splitting. *J. Phys. Chem. Lett.* **2019**, *10*, 3122–3128.
- (57) Martyna, G. J.; Klein, M. L.; Tuckerman, M. Nosé-Hoover chains: The canonical ensemble via continuous dynamics. *J. Chem. Phys.* **1992**, *97*, 2635.